Chinese Journal of Aeronautics, 2013,26(4): 1017–1028

Chinese Society of Aeronautics and Astronautics
& Beihang University

Chinese Journal of Aeronautics

cja@buaa.edu.cn
www.sciencedirect.com

Precise control of a magnetically suspended double-gimbal control moment gyroscope using differential geometry decoupling method

Chen Xiaocen [a,b,*], **Chen Maoyin** [a]

[a] *Department of Automation, Tsinghua University, Beijing 100084, China*
[b] *Department of Electronic and Optical Engineering, Ordnance Engineering College, Shijiazhuang 050003, China*

Received 7 June 2012; revised 23 October 2012; accepted 2 February 2013
Available online 2 July 2013

KEYWORDS

Differential geometry decoupling;
Dynamic compensation;
Internal model controller;
MSDGCMG;
Spacecraft control

Abstract Precise control of a magnetically suspended double-gimbal control moment gyroscope (MSDGCMG) is of vital importance and challenge to the attitude positioning of spacecraft owing to its multivariable, nonlinear and strong coupled properties. This paper proposes a novel linearization and decoupling method based on differential geometry theory and combines it with the internal model controller (IMC) to guarantee the system robustness to the external disturbance and parameter uncertainty. Furthermore, by introducing the dynamic compensation for the inner-gimbal rate-servo system and the magnetically suspended rotor (MSR) system only, we can eliminate the influence of the unmodeled dynamics to the decoupling control accuracy as well as save costs and inhibit noises effectively. The simulation results verify the nice decoupling and robustness performance of the system using the proposed method.

1. Introduction

Control moment gyroscope (CMG) is the key attitude control actuator of spacecraft.[1] Many countries such as America, Britain, Russia and France have attached much importance to this technology.

Generally speaking, CMG consists of two subsystems i.e., the high-speed rotor system and the gimbal rate-servo system. According to the different properties of bearing method, CMG can be classified as mechanical CMG and magnetically suspended CMG (MSCMG). Although simple in structure and control, mechanical CMG is easy to wear and vibrate. Magnetic bearing is complex, but it owns zero friction and wear as well as high potential of high control precision and long life span. On the other hand, according to different degrees-of-freedom (DOF) of gimbal rate-servo system, CMG can be divided into single-gimbal CMG (SGCMG) and double-gimbal CMG (DGCMG).[2,3] Compared to the SGCMG, the DGCMG can afford to control 2-DOF which definitely reduces the whole volume and weight of spacecraft. In view of the above-mentioned factors, a MSDGCMG (Magnetically Suspended Double Gimbal Control Moment Gyroscope) is becoming a preferred positioning actuator in the field of aerospace.[4]

MSCMG is a multivariable, nonlinear and strong coupled complex system with heavy gyroscopic effect and moving-

* Corresponding author at: Department of Automation, Tsinghua University, Beijing 100084, China. Tel.: +86 10 82888888.
E-mail address: xiaocen_88@sina.cn (X. Chen).

Peer review under responsibility of Editorial Committee of CJA.

Production and hosting by Elsevier

1000-9361 © 2013 Production and hosting by Elsevier Ltd. on behalf of CSAA & BUAA. Open access under CC BY-NC-ND license.
http://dx.doi.org/10.1016/j.cja.2013.06.010

gimbal effect, which presents a puzzling and challenging issue for its precise control. In the past decades, a number of control strategies have been studied to inhibit the gyroscopic effect and moving-gimbal effect. On the whole, there are two dominating kinds of methods. One is the coupled moment compensation method; the other is the linearization and decoupling (L&D) method.

Built upon the coupled moment compensation theory, some scholars propose the decentralized PID-cross feedback control method to inhibit the gyroscopic effect of a MSCMG[5] (Magnetically Suspended Control Moment Gyroscope). Given that the model is inaccurate due to approximate linearization errors, as well as it is difficult to debug and adjust parameters in practice, the decoupling effect and control accuracy are unsatisfactory. When it comes to solving the moving-gimbal effect, some researchers employ the angular velocity-current feedforward control method for a MSSGCMG[6] Magnetically Suspended Single Gimbal Control Moment Gyroscope). However, note that the modeling of the dynamic is too simplified, this proposal is unsatisfactory in realizing high-precision control. On account of the above factors, the original authors put forward the compound control method based on angular velocity feedback and the given angular acceleration feedforward to make modification.[7] Admitting that this way can realize good steady performance, it cannot achieve favorable dynamic properties induced by the errors between the practical angular acceleration and the given one. Further, even if taking the practical angular acceleration instead of the given one may resolve this issue in theory, it inevitably introduces heavy noises, which goes against practical implementation. Meanwhile, the nonlinearity and interaction moment between the MSR (Magnetically Suspended Rotor) system and the gimbal rate-servo system have been neglected in those methods which is endurable for a MSSGCMG, but is infeasible for a MSDGCMG since the moving-gimbal effect is much stronger and the nonlinearity of dynamic coupling is more complex and heavier. Together with the coupled moment compensation theory, the L&D theory has been developing prosperously. There is extensive literature discussing the decoupling method directed at the control issue of nonlinear systems, such as neural-networked decoupling method,[8–11] fuzzy decoupling method[12] and feedback L&D method. The intelligent decoupling method is desired if the system model is hard to identify, but is inferior in engineering application as it needs quantities of data, repetitive tests and large computational resources. For this reason, L&D method has been widely used.

Overall, L&D method can be sorted into two classes, one is the differential geometry decoupling method,[13–15] the other is the dynamic inverse decoupling method.[16–19]

With regard to the control issue of a MSSGCMG, J C Fang and Y Ren adopt a dynamic inverse decoupling method, and the simulation and experimental results show the effectiveness of this scheme.[20]

Up to now, there is rare literature concerning the control issue of the MSDGCMG. As for a MSDGCMG, though simply added one gimbal compared with the MSSGCMG, the coupling effects among the MSR system and the two gimbal rate-servo systems become much stronger and more complex, with strong nonlinearity. In particular, the nonlinear interaction moment between the two gimbal rate-servo systems multiplies difficulties of feedback linearization and decoupling. As a result, precise control of the dynamic system is confusing and challenging to realize the high-precision attitude positioning of a spacecraft.

It is worth noting that matching with the dynamic inverse decoupling method, the differential geometry decoupling method is more conductive for the theory deployment and we can lucubrate more widely. Hence, the differential geometry theory is explored in this paper.

In virtue of large dependence of exact L&D theory on the mathematical model accuracy, the phase lag induced by the unmodeled dynamics inevitably affects the decoupling performance. To resolve this problem as well as avoid causing excessive computational resources and bringing in heavy noises, dynamic compensation for the inner gimbal rate-servo system and the MSR system is added to the dynamic system.

Besides, IMC is prominent over traditional PID controller in achieving satisfactory static and dynamic performances. To improve the system robustness, we adopt the differential geometry decoupling plus IMC method to obtain the high-accuracy control of the MSDGCMG.

This paper is organized as follows. First, in Section 2, we construct the model of a MSDGCMG and analyze its dynamic characteristics. After that, a differential geometry decoupling method based on current mode and design of dynamic compensation as well as robust controller is specified in Section 3. Then, the comparative simulations between the proposed method and the traditional one are carried out in Section 4. Finally, Section 5 concludes the paper.

2. Modeling and characteristics analysis of MSDGCMG

2.1. Modeling of MSDGCMG

The operating principle of a MSDGCMG is that the high-speed MSR system supplies constant angular momentum, and the gimbal rate-servo system rotation changes the direction of the angular momentum to output gyro torque. Fig. 1 shows the structure and coordinates of the MSR system in a MSDGCMG.[20]

The rotor is suspended by two 2-DOF radial magnetic bearings, and two single-DOF axial magnetic bearings. O is the geometric center of the magnetic bearing stator. G and m is the gravity and mass of the magnetic bearing. Ω is the rotor speed. X, Y and Z axes form the generalized coordinates of the rotor position, f_x and f_y are the magnetic forces in the X and Y axes, x and y denote the linear displacements of rotor

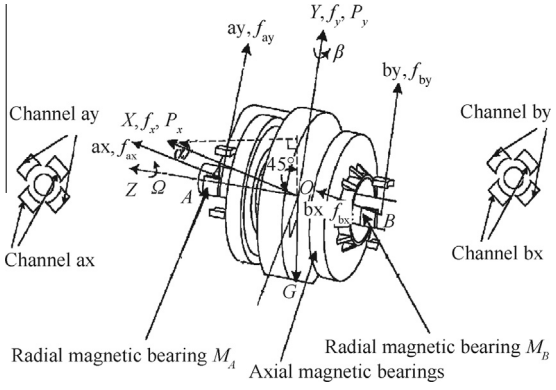

Fig. 1 Structure and coordinates of MSR system in a MSDGCMG.[20]

from the center O in the X and Y axes, P_x and P_y are the output torques in the X and Y axes, α and β are the rotational angles relative to the X and Y axes. M_A and M_B represent the radial magnetic bearings in the two ends A and B, respectively. f_{ax}, f_{ay}, f_{bx} and f_{by} are the magnetic forces along the magnetic coordinates ax, ay, bx and by axes, h_{ax}, h_{ay}, h_{bx} and h_{by} are the linear displacements of rotor from the center O along the magnetic bearing coordinates. J_{rr} denotes the moment of inertia of the MSR system along the radial magnetic coordinates. l_m denotes the distance from the point of magnetic force along the radial magnetic coordinates to the geometric center of rotor. H_{rz} represents the angular momentum of the MSR system. And H_{rz} delegates the norm of the vector. For the sake of full use of magnetic forces to control rotor, we often install radial stators in 45°. Simultaneously, we can simplify the magnetic force-current/position stiffness by the variable operating-point linearization method. In other words, the magnetic force can be described as follows:

$$f_\lambda = K_{i\lambda} i_\lambda + K_{h\lambda} h_\lambda \quad (\lambda = \mathrm{ax}, \mathrm{ay}, \mathrm{bx}, \mathrm{by}) \tag{1}$$

where $K_{i\lambda}$ and $K_{h\lambda}$ represent the current/position stiffness of the MSR system, and i_λ represents drive current along the radial magnetic bearing.

The relationship between the current stiffness and the current is symmetrical as well as the one between the displacement stiffness and the displacement. Moreover, the current of the four radial channels are symmetrical under the normal operating conditions. That is to say, the current stiffness of the four channels is roughly identical with each other. Likewise, the displacement stiffness of the four channels is roughly the same with each other. Therefore we can substitute K_i for $K_{i\lambda}$, and K_h for $K_{h\lambda}$.

When we talk about the gimbal rate-servo systems, θ_g and θ_j represent the rotational angles, K_{igx} and K_{ijy} denote the current stiffness, i_{gx} and i_{jy} mean the drive current in the output torque direction, and P_{gx} and P_{jy} demonstrate the output torques of inner and outer gimbal rate-servo systems separately. J_{gx}, J_{gy} and J_{gz} represent the moments of inertia along the coordinates of the inner gimbal rate-servo system. J_{jy} represents the moment of inertia in the output torque direction of the outer gimbal rate-servo system.

On the basis of Euler equation, we can get the model of a MSDGCMG as follows:

$$m\ddot{x} = f_{\mathrm{ax}} + f_{\mathrm{bx}} \tag{2}$$

$$m\ddot{y} = f_{\mathrm{ay}} + f_{\mathrm{by}} \tag{3}$$

$$J_{rr}\left(\frac{\sqrt{2}}{2}\ddot{\theta}_j \cos\theta_g - \frac{\sqrt{2}}{2}\dot{\theta}_j\dot{\theta}_g \sin\theta_g + \frac{\sqrt{2}}{2}\ddot{\theta}_g + \ddot{\alpha}\right) + H_{rz}\left(\frac{\sqrt{2}}{2}\dot{\theta}_j \cos\theta_g - \frac{\sqrt{2}}{2}\dot{\theta}_g + \dot{\beta}\right) = P_x \tag{4}$$

$$J_{rr}\left(\frac{\sqrt{2}}{2}\ddot{\theta}_j \cos\theta_g - \frac{\sqrt{2}}{2}\dot{\theta}_j\dot{\theta}_g \sin\theta_g - \frac{\sqrt{2}}{2}\ddot{\theta}_g + \ddot{\beta}\right) - H_{rz}\left(\frac{\sqrt{2}}{2}\dot{\theta}_j \cos\theta_g + \frac{\sqrt{2}}{2}\dot{\theta}_g + \dot{\alpha}\right) = P_y \tag{5}$$

$$J_{gx}\ddot{\theta}_g - (J_{gz} - J_{gy})\dot{\theta}_j^2 \sin\theta_g \cos\theta_g + \frac{\sqrt{2}}{2}(P_x - P_y) = P_{gx} \tag{6}$$

$$J_{gy}(\ddot{\theta}_j \cos\theta_g - \dot{\theta}_j\dot{\theta}_g \sin\theta_g) - (J_{gx} - J_{gz})\dot{\theta}_j\dot{\theta}_g \sin\theta_g + \frac{\sqrt{2}}{2}(P_x + P_y) = P_{gy} \tag{7}$$

$$-J_{gz}\ddot{\theta}_j \sin\theta_g + (J_{gy} - J_{gx} - J_{gz})\dot{\theta}_j\dot{\theta}_g \cos\theta_g = P_{gz} \tag{8}$$

$$J_{jy}\ddot{\theta}_j + P_{gy}\cos\theta_g - P_{gz}\sin\theta_g = P_{jy} \tag{9}$$

where

$$P_x = l_m(f_{\mathrm{by}} - f_{\mathrm{ay}}) \tag{10}$$

$$P_y = l_m(f_{\mathrm{ax}} - f_{\mathrm{bx}}) \tag{11}$$

$$P_{gx} = K_{igx} i_{gx} \tag{12}$$

$$P_{jy} = K_{ijy} i_{jy} \tag{13}$$

$$h_{\mathrm{ax}} = x + l_m\beta \tag{14}$$

$$h_{\mathrm{bx}} = x - l_m\beta \tag{15}$$

$$h_{\mathrm{ay}} = y - l_m\alpha \tag{16}$$

$$h_{\mathrm{by}} = y + l_m\alpha \tag{17}$$

2.2. Characteristics analysis of MSDGCMG

From Eq. (4), we discover that the output torque in X axe of MSR system P_x is associated with the rotational angles α and β relative to X and Y axes. Here,

$$\alpha = \frac{h_{\mathrm{by}} - h_{\mathrm{ay}}}{2l_m} \tag{18}$$

$$\beta = \frac{h_{\mathrm{ax}} - h_{\mathrm{bx}}}{2l_m} \tag{19}$$

So P_x is related with h_{ax}, h_{bx}, h_{ay} and h_{by}, which implies that four radial channels of the MSR system are coupled with each other. Meanwhile P_x is concerned with θ_j and θ_g, which signifies the MSR system is coupled with the two gimbal rate-servo systems also. The similar conclusion can be drawn from the output torque in Y axe of the MSR system P_y. From Eqs. (4)–(9) and (14)–(17) we can deduce the following expressions:

$$J_{gx}\ddot{\theta}_g + (J_{gy} - J_{gz})\dot{\theta}_j^2 \sin\theta_g \cos\theta_g + H_{rz}\left[\dot{\theta}_j \cos\theta_g + \frac{\sqrt{2}}{2}\left(\frac{\dot{h}_{\mathrm{by}} - \dot{h}_{\mathrm{ay}}}{2l_m} + \frac{\dot{h}_{\mathrm{ax}} - \dot{h}_{\mathrm{bx}}}{2l_m}\right)\right] + J_{rr}\left[\frac{\sqrt{2}}{2}\left(\frac{\ddot{h}_{\mathrm{by}} - \ddot{h}_{\mathrm{ay}}}{2l_m} - \frac{\ddot{h}_{\mathrm{ax}} - \ddot{h}_{\mathrm{bx}}}{2l_m}\right) + \ddot{\theta}_g\right] = P_{gx} \tag{20}$$

$$(J_{jy} + J_{gy}\cos^2\theta_g + J_{gz}\sin^2\theta_g + J_{rr}\cos^2\theta_g)\ddot{\theta}_j + J_{rr}\left[\frac{\sqrt{2}}{2}\left(\frac{\ddot{h}_{\mathrm{by}} - \ddot{h}_{\mathrm{ay}}}{2l_m} + \frac{\ddot{h}_{\mathrm{ax}} - \ddot{h}_{\mathrm{bx}}}{2l_m}\right)\cos\theta_g - \dot{\theta}_j\dot{\theta}_g \sin\theta_g \cos\theta_g\right] - H_{rz}\left[\frac{\sqrt{2}}{2}\left(\frac{\dot{h}_{\mathrm{by}} - \dot{h}_{\mathrm{ay}}}{2l_m} - \frac{\dot{h}_{\mathrm{ax}} - \dot{h}_{\mathrm{bx}}}{2l_m}\right) + \dot{\theta}_g\right]\cos\theta_g - 2(J_{gy} - J_{gz})\dot{\theta}_g\dot{\theta}_j \sin\theta_g \cos\theta_g = P_{jy} \tag{21}$$

Take inner gimbal rate-servo system as an example, we can discover that P_{gx} is bound up with h_{ax}, h_{bx}, h_{ay}, h_{by}, θ_g, θ_j and their derivatives, attesting that the inner gimbal rate-servo system is not only connected with the four radial channels of the MSR system, but also with the outer gimbal rate-servo system. The output torque of the outer gimbal rate-servo system P_{jy} agrees well with the same conclusion. In addition, the above formulas include trigonometric and quadratic functions, which prove that dynamics are interacted nonlinearly.

The above analysis boils down to the point that the MSDGCMG is a multivariable, nonlinear, and strong coupled system with heavy gyroscopic effect and moving-gimbal effect.

3. Differential geometry decoupling method based on current mode and design of dynamic compensation as well as robust controller

3.1. Precise linearization of MSDGCMG

First, we define the state variable $\boldsymbol{X}$, input variable $\boldsymbol{U}$, and output variable $\boldsymbol{Y}$:

$$\boldsymbol{X} = [\,x \quad y \quad \alpha \quad \beta \quad \theta_g \quad \theta_j \quad \dot{x} \quad \dot{y} \quad \dot{\alpha} \quad \dot{\beta} \quad \dot{\theta}_g \quad \dot{\theta}_j\,]^{\mathrm{T}}$$
$$\boldsymbol{U} = [\,i_{\mathrm{ax}} \quad i_{\mathrm{bx}} \quad i_{\mathrm{ay}} \quad i_{\mathrm{by}} \quad i_{gx} \quad i_{jy}\,]^{\mathrm{T}}$$
$$\boldsymbol{Y} = [\,h_{\mathrm{ax}} \quad h_{\mathrm{bx}} \quad h_{\mathrm{ay}} \quad h_{\mathrm{by}} \quad \theta_g \quad \theta_j\,]^{\mathrm{T}}$$

The nonlinear system can be inferred as an affine nonlinear system:

$$\begin{cases} \dot{\boldsymbol{X}} = \boldsymbol{f}(\boldsymbol{X}) + \boldsymbol{g}(\boldsymbol{X})\boldsymbol{U} \\ \boldsymbol{Y} = \boldsymbol{h}(\boldsymbol{X}) \end{cases} \tag{22}$$

where $\boldsymbol{f}(\boldsymbol{X})$, $\boldsymbol{g}(\boldsymbol{X})$ and $\boldsymbol{h}(\boldsymbol{X})$ are shown in the appendix.

It can be perceived that the system is a six-input, six-output nonlinear system, and the relative order can be calculated as follows:

$$L_{g_j}\boldsymbol{h}_i(\boldsymbol{X}) = 0 \quad (i,j = 1,2,\ldots,6) \tag{23}$$

In accordance with the differential geometry theory,[21]

$$\begin{aligned} \dot{y}_i &= \frac{\partial \boldsymbol{h}_i(\boldsymbol{X})}{\partial \boldsymbol{X}}\dot{X} = \frac{\partial \boldsymbol{h}_i(\boldsymbol{X})}{\partial \boldsymbol{X}}[\boldsymbol{f}(\boldsymbol{X}) + \boldsymbol{g}(\boldsymbol{X})\boldsymbol{U}] \\ &= \frac{\partial \boldsymbol{h}_i(\boldsymbol{X})}{\partial \boldsymbol{X}}f(\boldsymbol{X}) + \frac{\partial \boldsymbol{h}_i(\boldsymbol{X})}{\partial \boldsymbol{X}}\boldsymbol{g}(\boldsymbol{X})\boldsymbol{U} \\ &= \boldsymbol{L}_f\boldsymbol{h}_i(\boldsymbol{X}) + \sum_{j=1}^{m}\boldsymbol{L}_{g_j}\boldsymbol{h}_i(\boldsymbol{X})\boldsymbol{U}_j \end{aligned} \tag{24}$$

If $L_{g_j}\boldsymbol{h}_i(\boldsymbol{X}) = 0$ for any j, Eq. (24) should be differentiated once more. By means of differentiation, we can obtain the matrix $\boldsymbol{A}(\boldsymbol{X})$ and $\boldsymbol{B}(\boldsymbol{X})$ as formulated in the appendix. Furthermore,

$$\det(\boldsymbol{A}(\boldsymbol{X})) = \frac{16K_i^3K_{igx}K_{ijy}}{m^3J_{gx}^2\cos x_5}\left(\frac{2K_il_m^2}{J_{rr}} + \frac{K_il_m^2\cos^2 x_5}{\eta} + \frac{K_il_m^2}{J_{gx}}\right) \neq 0 \tag{25}$$

Where det means determinant notation, $\eta = J_{jy} + J_{gy}\cos^2 x_5 + J_{gz}\sin^2 x_5$ and $x_5 = \theta_g$.

Accordingly, the system can be exactly linearized using feedback linearization theory.

Define new variables to substitute for the second derivatives of the original output variables. Namely,

$$[\,v_1 \quad v_2 \quad v_3 \quad v_4 \quad v_5 \quad v_6\,]^{\mathrm{T}} = [\,\ddot{y}_1 \quad \ddot{y}_2 \quad \ddot{y}_3 \quad \ddot{y}_4 \quad \ddot{y}_5 \quad \ddot{y}_6\,]^{\mathrm{T}}$$

The above equation can be yielded:

$$\begin{aligned} &[\,v_1 \quad v_2 \quad v_3 \quad v_4 \quad v_5 \quad v_6\,]^{\mathrm{T}} \\ &= \boldsymbol{B}(\boldsymbol{X}) + \boldsymbol{A}(\boldsymbol{X})[\,u_1 \quad u_2 \quad u_3 \quad u_4 \quad u_5 \quad u_6\,]^{\mathrm{T}} \end{aligned} \tag{26}$$

In turn, the nonlinear control law can be derived from Eq. (26):

$$\begin{aligned} [\,u_1 \quad u_2 \quad u_3 \quad u_4 \quad u_5 \quad u_6\,]^{\mathrm{T}} &= -\boldsymbol{A}^{-1}(\boldsymbol{X})\boldsymbol{B}(\boldsymbol{X}) + \boldsymbol{A}^{-1}(\boldsymbol{X}) \\ &\quad [\,v_1 \quad v_2 \quad v_3 \quad v_4 \quad v_5 \quad v_6\,]^{\mathrm{T}} \end{aligned} \tag{27}$$

Plugging $\boldsymbol{A}(\boldsymbol{X})$ and $\boldsymbol{B}(\boldsymbol{X})$ into Eq. (27), we can receive the clear expressions of the control laws:

$$\begin{aligned} u_1 = \frac{1}{2l_mK_i}\Bigg[&\frac{ml_m(v_1+v_2)}{2} - H_{rz}\left(\frac{\sqrt{2}}{2}x_{12}\cos x_5 + \frac{\sqrt{2}}{2}x_{11} + x_9\right) \\ &-2K_hl_m(x_1 + l_mx_4) + J_{rr}\left(\frac{\sqrt{2}}{2}v_6\cos x_5 - \frac{\sqrt{2}}{2}x_{11}x_{12}\sin x_5\right. \\ &\left.-\frac{\sqrt{2}}{2}v_5 + \frac{v_1 - v_2}{2l_m}\right)\Bigg] \end{aligned} \tag{28}$$

$$\begin{aligned} u_2 = \frac{1}{2l_mK_i}\Bigg[&\frac{ml_m(v_1+v_2)}{2} + H_{rz}\left(\frac{\sqrt{2}}{2}x_{12}\cos x_5 + \frac{\sqrt{2}}{2}x_{11} + x_9\right) \\ &-2K_hl_m(x_1 - l_mx_4) - J_{rr}\left(\frac{\sqrt{2}}{2}v_6\cos x_5 - \frac{\sqrt{2}}{2}x_{11}x_{12}\sin x_5\right. \\ &\left.-\frac{\sqrt{2}}{2}v_5 + \frac{v_1 - v_2}{2l_m}\right)\Bigg] \end{aligned} \tag{29}$$

$$\begin{aligned} u_3 = \frac{1}{2l_mK_i}\Bigg[&\frac{ml_m(v_3+v_4)}{2} - H_{rz}\left(\frac{\sqrt{2}}{2}x_{12}\cos x_5 + \frac{\sqrt{2}}{2}x_{11} + x_{10}\right) \\ &-2K_hl_m(x_2 - l_mx_3) - J_{rr}\left(\frac{\sqrt{2}}{2}v_6\cos x_5 - \frac{\sqrt{2}}{2}x_{11}x_{12}\sin x_5\right. \\ &\left.-\frac{\sqrt{2}}{2}v_5 + \frac{v_4 - v_3}{2l_m}\right)\Bigg] \end{aligned} \tag{30}$$

$$\begin{aligned} u_4 = \frac{1}{2l_mK_i}\Bigg[&\frac{ml_m(v_3+v_4)}{2} + H_{rz}\left(\frac{\sqrt{2}}{2}x_{12}\cos x_5 - \frac{\sqrt{2}}{2}x_{11} + x_{10}\right) \\ &-2K_hl_m(x_2 + l_mx_3) + J_{rr}\left(\frac{\sqrt{2}}{2}v_6\cos x_5 - \frac{\sqrt{2}}{2}x_{11}x_{12}\sin x_5\right. \\ &\left.-\frac{\sqrt{2}}{2}v_5 + \frac{v_4 - v_3}{2l_m}\right)\Bigg] \end{aligned} \tag{31}$$

$$\begin{aligned} u_5 = \frac{1}{K_{igx}}\Bigg[&J_{gx}v_5 + \lambda_3 + H_{rz}\left(x_{12}\cos x_5 + \frac{\sqrt{2}}{2}(x_9 + x_{10})\right) \\ &+J_{rr}\left[\frac{\sqrt{2}}{2}\left(\frac{v_4 - v_3}{2l_m} - \frac{v_1 - v_2}{2l_m}\right) + v_5\right]\Bigg] \end{aligned} \tag{32}$$

$$\begin{aligned} u_6 = \frac{1}{K_{ijy}}\Bigg[&\lambda_2v_6 + J_{rr}\left[\frac{\sqrt{2}}{2}\left(\frac{v_4 - v_3}{2l_m} + \frac{v_1 - v_2}{2l_m}\right)\cos x_5\right] \\ &-\lambda_1 - H_{rz}\left[\frac{\sqrt{2}}{2}(x_9 - x_{10}) + x_{11}\right]\cos x_5 \\ &-J_{rr}x_{11}x_{12}\sin x_5\cos x_5\Bigg] \end{aligned} \tag{33}$$

where

$$\begin{cases} \lambda_1 = 2(J_{gy} - J_{gz})x_{11}x_{12}\sin x_5 \cos x_5 \\ \lambda_2 = J_{jy} + J_{gy}\cos^2 x_5 + J_{gz}\sin^2 x_5 \\ \lambda_3 = (J_{gz} - J_{gy})x_{12}^2 \sin x_5 \cos x_5 \end{cases}.$$

3.2. Dynamic compensation

Mention that the power amplifier is necessary in practice, which inescapably results in the phase lag, leads to the control signal delay, and will further deteriorate the system decoupling accuracy. To alleviate the phase lag, we introduce the dynamic compensation into the system.

Primarily, the phase lag of the MSR system not only influences the decoupling effect but also endangers the nutation stability of the MSR system itself. Consequently, the dynamic compensation for the MSR system is indispensable.

As for the gimbal rate-servo system, there is no doubt that the problem of phase lag can be resolved more thoroughly by introducing dynamic compensation into both the inner and outer gimbal rate-servo systems. However, this measure will inevitably bring heavy noises and consume large computational resources to the extent of affecting the implementation of the control strategy and control performance. To settle this problem, coupling characteristics of two gimbal rate-servo systems are further analyzed.

The model of the dynamics yields the following equations:

$$\ddot{\theta}_g = \frac{\left\{K_{igx}i_{gx} + (J_{gz} - J_{gy})\dot{\theta}_j^2 \sin\theta_g \cos\theta_g - \frac{\sqrt{2}}{2}\left[2K_h l_m^2\left(\frac{h_{by} - h_{ay}}{2l_m} - \frac{h_{ax} - h_{bx}}{2l_m}\right) + 2K_i l_m\left(\frac{i_{by} - i_{ay}}{2} - \frac{i_{ax} - i_{bx}}{2}\right)\right]\right\}}{J_{gx}} \tag{34}$$

$$\ddot{\theta}_j = \frac{\left\{K_{ijy}i_{jy} + 2(J_{gy} - J_{gz})\dot{\theta}_g\dot{\theta}_j \sin\theta_g \cos\theta_g - \frac{\sqrt{2}}{2}\left[2K_i l_m\left(\frac{i_{by} - i_{ay}}{2} + \frac{i_{ax} - i_{bx}}{2}\right) + 2K_h l_m^2\left(\frac{h_{by} - h_{ay}}{2l_m} + \frac{h_{ax} - h_{bx}}{2l_m}\right)\right]\cos\theta_g\right\}}{J_{jy} + J_{gy}\cos^2\theta_g + J_{gz}\sin^2\theta_g} \tag{35}$$

Based on Eqs. (34) and (35), we find that the coupling effect between the outer gimbal rate-servo system and the MSR system is in proportion to the cosine function of the rotational angle of inner gimbal rate-servo system, and the denominator in Eq. (35) is larger than that in Eq. (34), both of which indicate that the coupling effect between the inner gimbal rate-servo system and the MSR system is larger than that between the outer gimbal rate-servo system and the MSR system. Of course, we expect to decouple the MSDGCMG as thoroughly as possible as well as save costs and reduce noises. To approach this, we merely add the dynamic compensation into the four radial channels of the MSR system and the inner gimbal rate-servo system.

The simplified structure of the amplifier is shown in Fig. 2.[22]

Where i_r represents the reference input current, and i delegates the actual output current. k_p is the amplification factor, and k_f is the feedback factor of current loop. $e^{-\tau s}$ denotes the delay link, and R and L represent the resistor and inductance of the coil respectively. And the transfer function of the delay link $e^{-\tau s}$ can be obtained via the first order Tailor expansion:

$$e^{-\tau s} = \frac{1}{1 + \tau s} \tag{36}$$

Then, the transfer function of the closed-loop control system can be simplified as follows:

$$G_a(s) \approx \frac{k_p}{L\tau s^2 + (L + R\tau)s + R + k_p k_f} \tag{37}$$

The phase lag of the MSR system at the rated nutation frequency can be removed in line with the Bode plot. Combined with the nutation stability criterion of the MSR system,[23] we can work out the minimum phase needed to be compensated. As far as the inner gimbal rate-servo system is concerned, the transfer function of the amplifier is the same as above. Similarly can we construct lead compensation for the lag part. In theory, the higher the order of the dynamic compensation, the more exact the compensation for the phase lag. But in view of the inconvenience in physical realization of high-order differentiation and the fact that it will bring heavy noises, we usually adopt the first-order high-pass filter:

$$C_f(s) = \frac{(L + R\tau)s + R + k_p k_f}{k_p} \tag{38}$$

To reject the system noises, incomplete derivative is employed to replace the first derivative. That is to say, $s \approx s/(1 + ks)$, where k is a small constant.

$$C_f(s) = \frac{(L + R\tau)\dfrac{s}{1 + ks} + R + k_p k_f}{k_p} \tag{39}$$

Considering the bandwidth and noise depression, we choose $k = 0.0001$.

Fig. 3 shows the contrast frequency characteristic of dynamic compensation for the inner gimbal rate-servo system. The dotted lines denote the curves before dynamic compensation and the real lines denote the opposite.

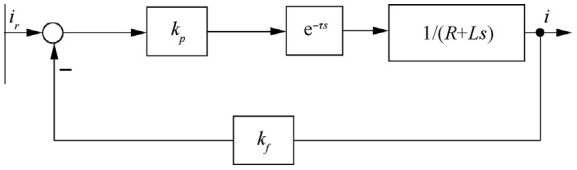

Fig. 2 Simplified structure of a power amplifier.

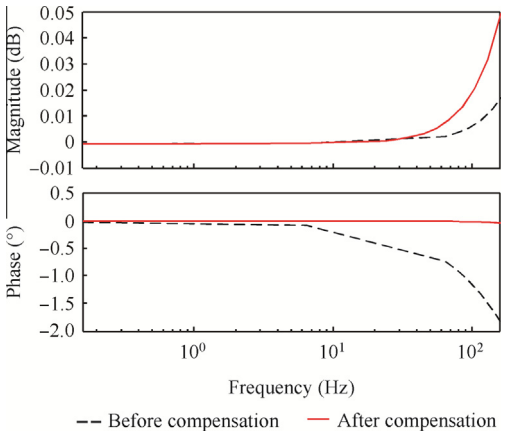

Fig. 3 Contrast frequency characteristic of dynamic compensation for inner gimbal rate-servo system.

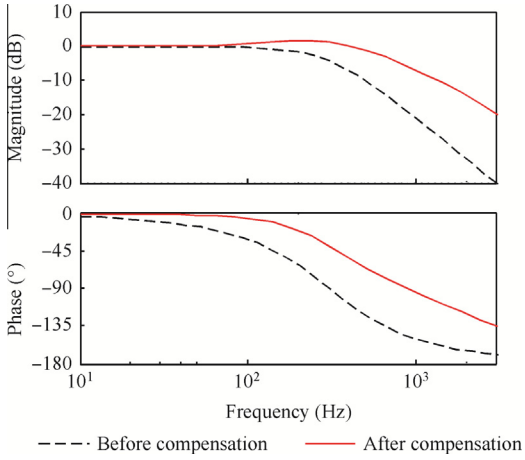

Fig. 4 Contrast frequency characteristic of dynamic compensation for MSR system.

From Fig. 3, we can discover that after employing the dynamic compensation filter for the inner gimbal rate-servo system, the phase compensation in the low-frequency is obvious while the amplitude increases little, which contribute to improving the decoupling performance and inhibit the negative influence of noise on the current sampling accuracy.

Fig. 4 shows the contrast frequency characteristic of dynamic compensation for MSR system. For MSR system, its rated rotor speed is 20000 r/min, and its rated nutation frequency needed to be controlled is about 600 Hz. From Fig. 4, it can be drawn that both the phase lag and amplitude attenuation at 600 Hz have been effectively compensated by the dynamic compensation filters.

3.3. Robust controller design

In the actual control system, due to the objective reality of model error and external disturbance, the differential geometry decoupling method cannot realize the complete linearization and decoupling of the controlled plant. Thus, in order to inhibit the influence of the residual coupling and nonlinearity to the system performance, it is necessary to adopt robust controller on the decoupled pseudolinear system. 2-DOF IMC(Internal Model Controller)[20] can realize independent control of tracking, disturbance rejection and robustness to the parameter uncertainty so as to achieve the unity of tracking and robustness. Meanwhile, it is quite easy for engineering implementation. Therefore, we employ IMC to realize setting and synthesis of the system.

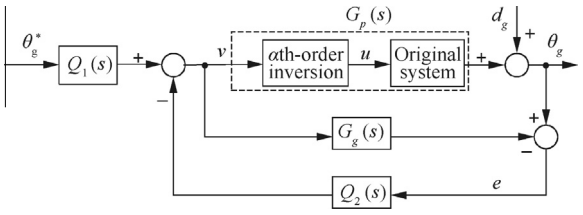

Fig. 5 Structure of the 2-DOF IMC.

Take inner gimbal rate-servo system as an example, its pseudolinear subsystem is:

$$G_g(s) = 1/s^2 \tag{40}$$

Considering the parameter uncertainty and model errors, the composition of the physical object and its inversion is not exactly equivalent to the linear subsystem. The plant, including uncertainties, can be written as

$$G_p(s) = G_g(s) + \Delta G(s) \tag{41}$$

where $\Delta G(s)$ is within the certain limitation.

Fig. 5 shows the closed-loop structure, including the 2-DOF IMC for inner gimbal rate-servo system.

Where $\theta_g^*(s)$ represents the reference-input angle of inner gimbal rate-servo system, e represents the error between desired and actual outputs, and d_g represents the outer disturbance.

From Fig. 5, the output is given by

$$\theta_g(s) = G_g(s)Q_1(s)\theta_g^*(s) + (1 - Q_2(s)G_g(s))d_g(s) \tag{42}$$

It is obvious that the tracking performance only depends on $Q_1(s)$, while the disturbance rejection performance only relies upon $Q_2(s)$. In order to track the reference input without any steady-state error and to improve the system robustness, low-pass filters $F_1(s)$ and $F_2(s)$ are introduced into $Q_1(s)$ and $Q_2(s)$. Separately, we choose,

$$\begin{cases} Q_1(s) = F_1(s)/G_g(s) \\ Q_2(s) = F_2(s)/G_g(s) \end{cases} \tag{43}$$

Moreover,

$$\begin{cases} F_1(s) = 1/(\varepsilon_1 s + 1)^2 \\ F_2(s) = 1/(\varepsilon_2 s + 1)^2 \end{cases} \tag{44}$$

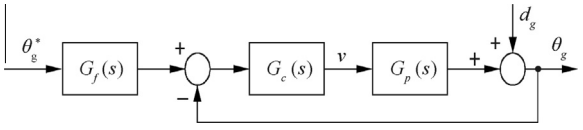

Fig. 6 Closed-loop system of 2-DOF IMC.

Hence, the improved IMC is shown as Fig. 6. Here

$$\begin{cases} G_f(s) = \dfrac{Q_1(s)}{Q_2(s)} = \dfrac{(\varepsilon_2 s+1)^2}{(\varepsilon_1 s+1)^2} \\ G_c(s) = \dfrac{Q_2(s)}{1-G_g(s)Q_2(s)} = \dfrac{s^2}{(\varepsilon_2 s+1)^2-1} \end{cases} \tag{45}$$

It can be proved that by choosing appropriate ε_2, we can achieve the stability of the closed-loop control system. Moreover, the bigger the ε_2, the bigger the $\Delta G(s)$ that can be tolerated. Further, the smaller the ε_1, the better the tracking characteristic. The smaller the ε_2, the better the robustness property. Correspondingly, under the allowing model error, we can realize the independent control of tracking and robustness properties by adjusting the parameters ε_1 and ε_2 (the robustness proof is detailed in Ref. [20]).

3.4. Control system overview

The control block diagram of MSDGCMG based on differential geometry decoupling plus IMC is shown in Fig. 7, where $C_{fm}(s)$ and $C_{fg}(s)$ are, respectively, the transfer functions of the dynamic compensation filters for the MSR system and inner gimbal rate-servo system.

Fig. 7 reveals that the original system connects with its inversion to form pseudolinear system, the transfer function of which is $1/s^2$. But the actual system includes unmodeled dynamics such as power amplifier and so on. Thus, to remove the negative influence of the unmodeled dynamics to the control accuracy, we need to add dynamic compensation before the power amplifier and original system which constitute generalized controlled plant. By means of the feedback linearization control, the controlled system turns to be the linear system. Due to the excellent robustness property of IMC, we adopt IMC to complete control task. The above is the principle of our innovative work.

Table 1 System parameters of a MSDGCMG.

Parameter	Value	Parameter	Value
m (kg)	15	l_m (m)	0.06253
K_i (N/A)	350	K_h (N/A)	8.5×10^5
K_{igx} (N/A)	0.84	K_{ijy} (N/A)	0.840
J_{rr} (kg·m^2)	0.062	J_z (kg·m^2)	0.1 019
J_{gx} (kg·m^2)	0.098	J_{gy} (kg·m^2)	0.297
J_{gz}(kg·m^2)	0.293	J_{jy} (kg·m^2)	0.722
R_g (Ω)	10.0	L_g(mH)	1.000
τ (μs)	333	R_m (Ω)	2.500
L_m (mH)	24.8		

4. Simulation results

In this section, comparative simulations between the traditional method (decentralized PID-cross plus compound control based on angular velocity feedback and angular acceleration feedforward) and the proposed one (differential geometry decoupling plus IMC) have been conducted. The system parameters are shown in Table 1, where R_m and L_m are the coil resistance and inductance of the radial magnetic bearings, and R_g and L_g are the circuit resistance and inductance of the inner gimbal servo motor.

4.1. Decoupling and tracking properties

Two comparative simulations are carried out to testify the decoupling and tracking performance of the proposed method.

Under the conditions that the rated rotor speed Ω = 20 000 r/min, at t = 0.2 s, the reference displacement of channel

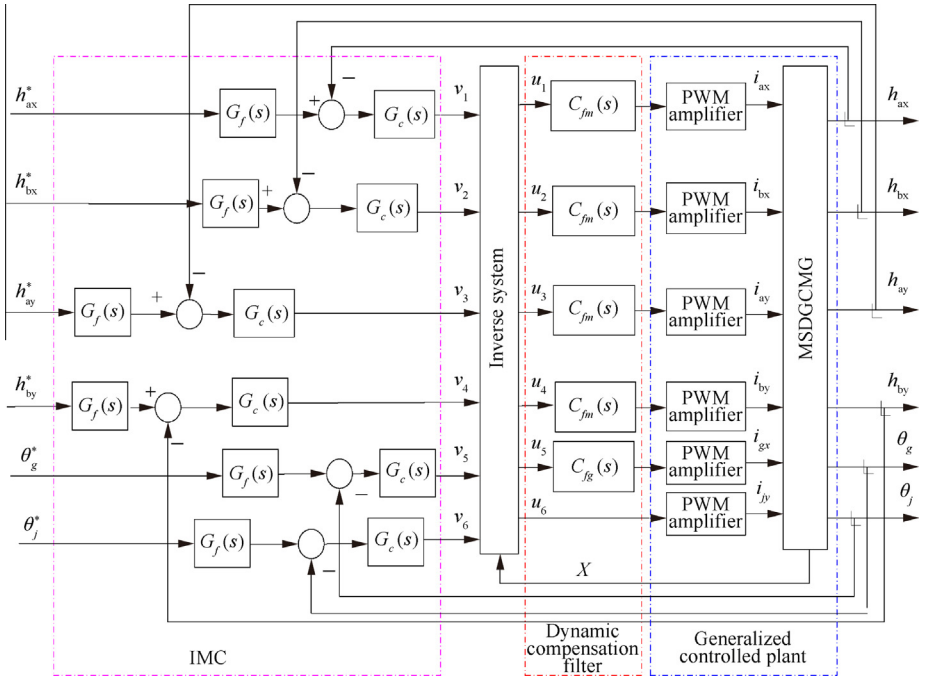

Fig. 7 Control block diagram of MSDGCMG based on differential geometry decoupling plus IMC.

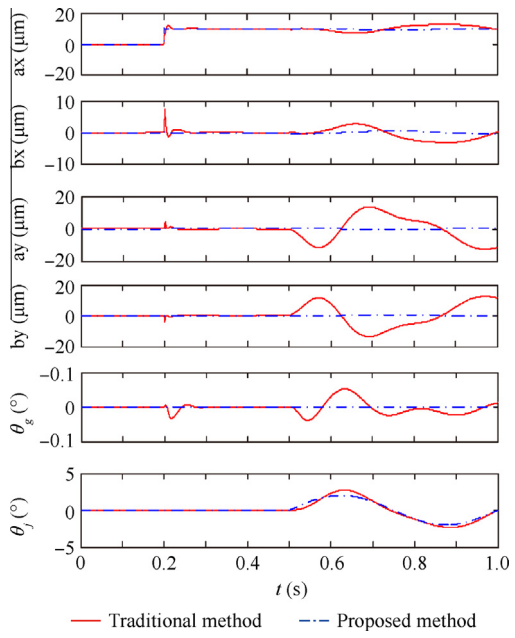

Fig. 8 Decoupling and tracking performance comparison using the traditional method and the proposed one.

ax steps from 0 to 10 μm and at $t = 0.5$ s, the outer gimbal rate-servo system receives the sinusoidal signal instruction, of which the amplitude is 2°, and the angular frequency is 2 Hz. The results are shown in Fig. 8, where the full and dotted lines denote the tracking curves of the traditional method and the proposed one separately.

From Fig. 8, we observe that concerning the traditional method, when the displacement of the channel ax steps from 0 to 10 μm at $t = 0.2$ s, there appears a range of overshoots among the four radial channels of the MSR system and the inner gimbal rate-servo system in varying degrees, with overstrike estimated at 2 μm in channels ax, ay and by, approximately 10 μm in channel bx, and around 0.04° in the inner gimbal rate-servo system. At once the outer gimbal rate-servo system operates sinusoidal motion at $t = 0.5$ s, there occurs coupling between the MSR system and the outer gimbal rate-servo system as well as the two gimbal rate-servo systems which conform to the conclusion we analyzed above. And the accommodation time is quite long. Meanwhile, the peak of the tracking curve of the outer-gimbal rate-servo system reaches 3°, exceeding the reference input. With respect to the novel method, the tracking curve adapts to the reference input very quickly and smoothly which proves the superiority of the proposed method.

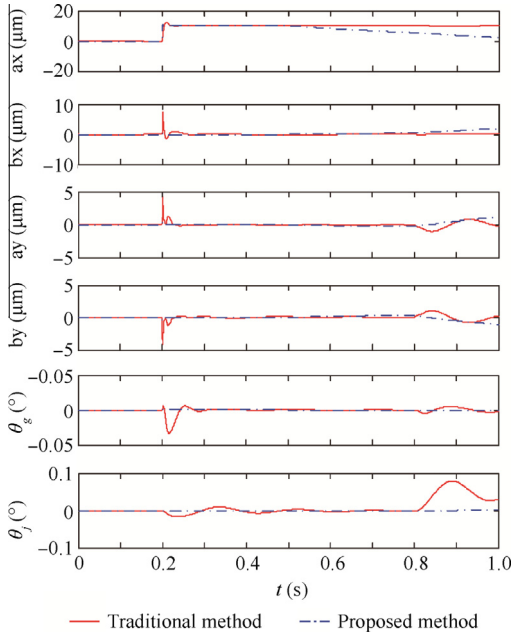

Fig. 9 Robustness performance comparison using the traditional method and the proposed one.

4.2. Robustness to external disturbance and parameter uncertainty

In order to test the robustness performance using the proposed method, we subject the two comparative simulations to the external disturbance and parameter variation.

Under the conditions that the rated rotor speed $\Omega = 20{,}000$ r/min, at $t = 0.2$ s, the displacement of channel ax in the MSR system steps from 0 to 10 μm, at $t = 0.5$ s, the current stiffness of the MSR system K_i changes from 350 to 380 N/A, then 1 N m size of torque is imposed on the outer gimbal rate-servo system at $t = 0.8$ s. Fig. 9 reveals the simulation results. Still, the full and dotted lines denote the tracking curves of the traditional method and the proposed one respectively.

According to Fig. 9, we can summarize that regarding the traditional method, there are deviations from the reference inputs among the other three channels of the MSR system as well as the two gimbal rate-servo systems at the time when the displacement of channel ax steps from 0 to 10 μm at $t = 0.2$ s. The deviation is especially large in channel bx which reaches 9 μm and is roughly −0.03° for the inner gimbal rate-servo system. Immediately the system is exposed to the external perturbation, the whole dynamics begin oscillation, partic-

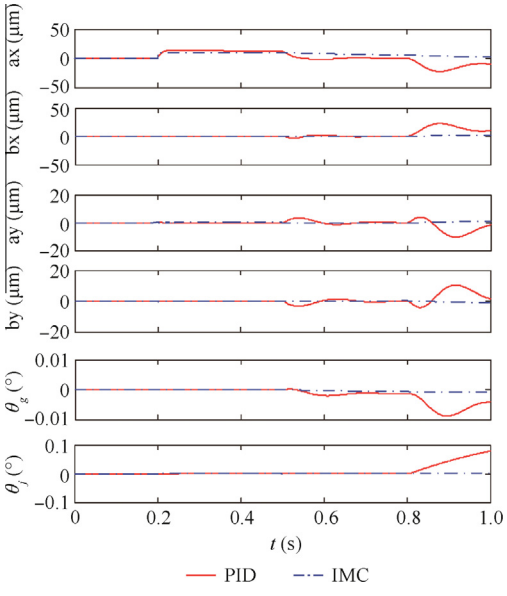

Fig. 10 Robustness performance comparison using differential geometry decoupling method plus PID controller and IMC.

ularly for the outer gimbal rate-servo system, with oscillation amplitude to 0.1°. On the contrary, the tracking curves of the proposed method are relatively steady with tiny fluctuation as soon as the reference input, parameter variation and external disturbance are forced on the system, showing the advantages in robustness property over the traditional method.

To further check the effectiveness of IMC, comparative simulations between the differential geometry decoupling plus PID controller and IMC are performed, and the results are shown in Fig. 10. Full and dotted lines stand for the tracking curves of the differential geometry decoupling plus PID controller and IMC separately. The simulation conditions are identical with above.

Fig. 10 points out that the tracking property of the system with PID controller is unsatisfactory immediately after the system accepts the reference input, parameter variation, and external disturbance. Evident in Fig. 10, on occasions when receiving the step signal, there emerges about 10 μm overshoot in channel ax. Subsequently, when the parameter changes at $t = 0.5$ s, the whole subsystems are affected in parallel. As the external disturbance comes along at $t = 0.8$ s, the tracking curve of the outer gimbal rate-servo system even diverges. However, the plot of the proposed method suggests the outstanding robustness property of the controlled plant.

4.3. Dynamic compensation effect

From the analysis above, we determine that dynamic compensation contributes to the precise control of MSDGCMG due to the phase lag caused by unmodeled dynamics. Meanwhile, the coupling effect between the outer gimbal rate-servo system and the MSR system is relatively small, and that's why we make suggestion merely to add dynamic compensation for the inner gimbal rate-servo system and the MSR system.

Thus, in this section, we alternatively introduce the dynamic compensation for the inner gimbal rate-servo system to perform comparative simulations on premise that dynamic compensation has been added into the MSR system. The simulation conditions are similar to those in Section 4.1 and the results are shown in Fig. 11. The full lines delegate the circumstance without the dynamic compensation, while the dotted lines delegate the opposite.

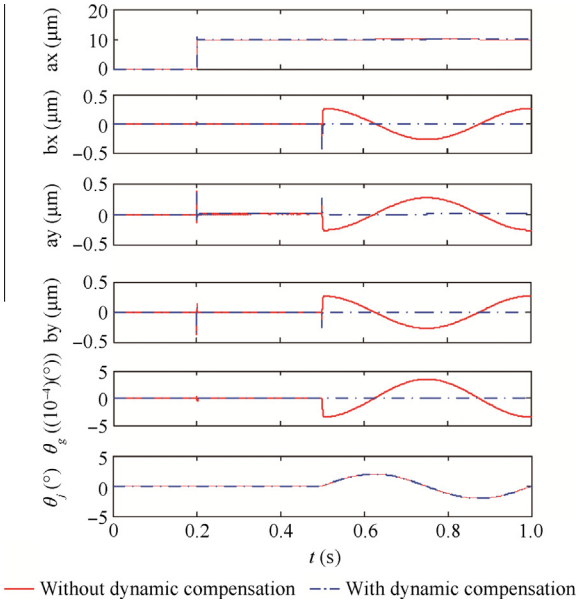

Fig. 11 Decoupling performance comparison of dynamic compensation for inner-gimbal rate-servo system.

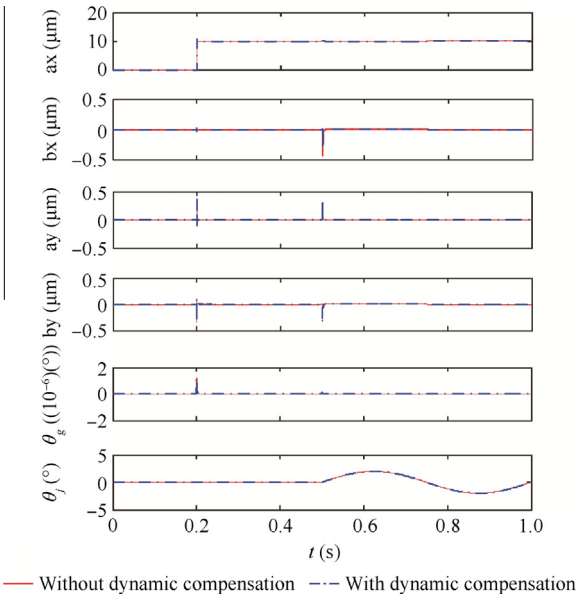

Fig. 12 Decoupling performance comparison of dynamic compensation for outer-gimbal rate-servo system.

Fig. 11 clarifies that the tracking curve without dynamic compensation for the inner gimbal rate-servo system is unwelcome when the outer gimbal rate-servo system receives the sinusoidal signal. There are significant coupling effects between the MSR system and the outer-gimbal rate-servo system as well as the two gimbal rate-servo systems, which is an indication of incomplete decoupling of the dynamic. Upon adding the dynamic compensation for the inner gimbal rate-servo system, the decoupling performance has been improved.

Moreover, it is requisite to verify there is no point in adding the dynamic compensation to the outer gimbal rate-servo system. We simulate two circumstances in which we alternately introduce the dynamic compensation for the outer gimbal rate-servo system on premise that five dynamic compensation units are equipped with the four radial channels of the MSR system as well as the inner gimbal rate-servo system. The simulation results are shown in Fig. 12.

From Fig. 12, we discover there is almost no distinction between the two tracking curves. The results prove the validity of the adopted measure, by which we are capable of decoupling the system completely as well as saving resources.

5. Conclusions

In order to precisely control a MSDGCMG, this paper proposes a differential geometry decoupling method based on current mode as well as introduces dynamic compensation plus IMC. The simulation results demonstrate that:

First, the proposed strategy can realize the exact linearization and decoupling of the MSDGCMG, avoiding the weakness of the traditional method.

Next, adding the dynamic compensation for the MSR system and the inner gimbal rate-servo system can not only effec-

tively improve the decoupling accuracy, eliminate the influence of the unmodeled dynamics to the decoupling accuracy, but also save computational resources and reject system noises.

Furthermore, IMC is better than PID controller in improving the robustness property of the controlled plant.

Acknowledgements

The authors wish to thank Prof. D.H. Zhou from Tsinghua University and Dr. Y. Ren from Beihang University for many valuable suggestions and instructive comments.

Appendix A

$$\boldsymbol{h}(\boldsymbol{X}) = [\, x_1 + l_m x_4 \quad x_1 - l_m x_4 \quad x_2 - l_m x_3 \quad x_2 + l_m x_3 \quad x_5 \quad x_6 \,]^T;$$

$$f(X) = \left[x_7 \;\; x_8 \;\; x_9 \;\; x_{10} \;\; x_{11} \;\; x_{12} \;\; \frac{2K_h x_1}{m} \;\; \frac{2K_h x_2}{m} \;\; \frac{2K_h l_m^2 x_3 - \Pi_1 - \Pi_2}{J_{rr}} \;\; \frac{2K_h l_m^2 x_4 + \Pi_3 - \Pi_4}{J_{rr}} \;\; \frac{\lambda_3 - \sqrt{2} K_h l_m^2 (x_3 - x_4)}{J_{gx}} \;\; \frac{\lambda_1 - \sqrt{2} K_h l_m^2 (x_3 + x_4)\cos x_5}{\lambda_2} \right]^T$$

where

$\lambda_1 = 2(J_{gy} - J_{gz}) x_{11} x_{12} \sin x_5 \cos x_5; \lambda_2 = J_{jy} + J_{gy} \cos^2 x_5 + J_{gz} \sin^2 x_5; \lambda_3 = (J_{gz} - J_{gy}) x_{12}^2 \sin x_5 \cos x_5 .$

$$\Pi_1 = H_{rz}\left(\frac{\sqrt{2}}{2} x_{12} \cos x_5 - \frac{\sqrt{2}}{2} x_{11} + x_{10}\right) - \frac{\sqrt{2}}{2} J_{rr} x_{11} x_{12} \sin x_5;$$

$$\Pi_2 = \frac{\sqrt{2}}{2} J_{rr} \cos x_5 \frac{\lambda_1 - \sqrt{2} K_h l_m^2 (x_3 + x_4)\cos x_5}{\lambda_2} + \frac{\sqrt{2}}{2} J_{rr} \frac{\lambda_3 - \sqrt{2} K_h l_m^2 (x_3 - x_4)}{J_{gx}};$$

$$\Pi_3 = H_{rz}\left(\frac{\sqrt{2}}{2} x_{12} \cos x_5 + \frac{\sqrt{2}}{2} x_{11} + x_9\right) + \frac{\sqrt{2}}{2} J_{rr} x_{11} x_{12} \sin x_5;$$

$$\Pi_4 = \frac{\sqrt{2}}{2} J_{rr} \cos x_5 \frac{\lambda_1 - \sqrt{2} K_h l_m^2 (x_3 + x_4)\cos x_5}{\lambda_2} - \frac{\sqrt{2}}{2} J_{rr} \frac{\lambda_3 - \sqrt{2} K_h l_m^2 (x_3 - x_4)}{J_{gx}}.$$

$$\boldsymbol{g}_1(\boldsymbol{X}) = \left[0 \;\; 0 \;\; 0 \;\; 0 \;\; 0 \;\; 0 \;\; \frac{K_i}{m} \;\; 0 \;\; \Pi_5 \;\; \Pi_6 \;\; \frac{\sqrt{2} K_i l_m}{2 J_{gx}} \;\; -\frac{\sqrt{2} K_i l_m \cos x_5}{2\lambda_2} \right]^T;$$

$$\boldsymbol{g}_2(\boldsymbol{X}) = \left[0 \;\; 0 \;\; 0 \;\; 0 \;\; 0 \;\; 0 \;\; \frac{K_i}{m} \;\; 0 \;\; -\Pi_5 \;\; -\Pi_6 \;\; -\frac{\sqrt{2} K_i l_m}{2 J_{gx}} \;\; -\frac{\sqrt{2} K_i l_m \cos x_5}{2\lambda_2} \right]^T;$$

$$\boldsymbol{g}_3(\boldsymbol{X}) = \left[0 \;\; 0 \;\; 0 \;\; 0 \;\; 0 \;\; 0 \;\; 0 \;\; \frac{K_i}{m} \;\; \Pi_7 \;\; \Pi_8 \;\; \frac{\sqrt{2} K_i l_m}{2 J_{gx}} \;\; \frac{\sqrt{2} K_i l_m \cos x_5}{2\lambda_2} \right]^T;$$

$$\boldsymbol{g}_4(\boldsymbol{X}) = \left[0 \;\; 0 \;\; 0 \;\; 0 \;\; 0 \;\; 0 \;\; 0 \;\; \frac{K_i}{m} \;\; -\Pi_7 \;\; -\Pi_8 \;\; -\frac{\sqrt{2} K_i l_m}{2 J_{gx}} \;\; -\frac{\sqrt{2} K_i l_m \cos x_5}{2\lambda_2} \right]^T;$$

$$\boldsymbol{g}_5(\boldsymbol{X}) = \left[0 \;\; 0 \;\; 0 \;\; 0 \;\; 0 \;\; 0 \;\; 0 \;\; 0 \;\; -\frac{\sqrt{2} K_{igx}}{2 J_{gx}} \;\; \frac{\sqrt{2} K_{igx}}{2 J_{gx}} \;\; \frac{K_{igx}}{J_{gx}} \;\; 0 \right]^T;$$

$$\boldsymbol{g}_6(\boldsymbol{X}) = \left[0 \;\; 0 \;\; 0 \;\; 0 \;\; 0 \;\; 0 \;\; 0 \;\; 0 \;\; -\frac{\sqrt{2}}{2} \cos x_5 \frac{K_{ijy}}{\lambda_2} \;\; -\frac{\sqrt{2}}{2} \cos x_5 \frac{K_{ijy}}{\lambda_2} \;\; 0 \;\; \frac{K_{ijy}}{\lambda_2} \right]^T;$$

Where

$$\Pi_5 = \frac{K_i l_m \cos^2 x_5}{2\lambda_2} - \frac{K_i l_m}{2J_{gx}}, \Pi_6 = \frac{K_i l_m}{J_{rr}} + \frac{K_i l_m \cos^2 x_5}{2\lambda_2} + \frac{K_i l_m}{2J_{gx}};$$

$$\Pi_7 = -\frac{K_i l_m}{J_{rr}} - \frac{K_i l_m \cos^2 x_5}{2\lambda_2} - \frac{K_i l_m}{2J_{gx}}, \Pi_8 = -\frac{K_i l_m \cos^2 x_5}{2\lambda_2} + \frac{K_i l_m}{2J_{gx}}.$$

$$\boldsymbol{A}(\boldsymbol{X}) = \begin{bmatrix} L_{g_1}L_f\boldsymbol{h}_1(\boldsymbol{X}) & L_{g_2}L_f\boldsymbol{h}_1(\boldsymbol{X}) & L_{g_3}L_f\boldsymbol{h}_1(\boldsymbol{X}) & L_{g_4}L_f\boldsymbol{h}_1(\boldsymbol{X}) & L_{g_5}L_f\boldsymbol{h}_1(\boldsymbol{X}) & L_{g_6}L_f\boldsymbol{h}_1(\boldsymbol{X}) \\ L_{g_1}L_f\boldsymbol{h}_2(\boldsymbol{X}) & L_{g_2}L_f\boldsymbol{h}_2(\boldsymbol{X}) & L_{g_3}L_f\boldsymbol{h}_2(\boldsymbol{X}) & L_{g_4}L_f\boldsymbol{h}_2(\boldsymbol{X}) & L_{g_5}L_f\boldsymbol{h}_2(\boldsymbol{X}) & L_{g_6}L_f\boldsymbol{h}_2(\boldsymbol{X}) \\ L_{g_1}L_f\boldsymbol{h}_3(\boldsymbol{X}) & L_{g_2}L_f\boldsymbol{h}_3(\boldsymbol{X}) & L_{g_3}L_f\boldsymbol{h}_3(\boldsymbol{X}) & L_{g_4}L_f\boldsymbol{h}_3(\boldsymbol{X}) & L_{g_5}L_f\boldsymbol{h}_3(\boldsymbol{X}) & L_{g_6}L_f\boldsymbol{h}_3(\boldsymbol{X}) \\ L_{g_1}L_f\boldsymbol{h}_4(\boldsymbol{X}) & L_{g_2}L_f\boldsymbol{h}_4(\boldsymbol{X}) & L_{g_3}L_f\boldsymbol{h}_4(\boldsymbol{X}) & L_{g_4}L_f\boldsymbol{h}_4(\boldsymbol{X}) & L_{g_5}L_f\boldsymbol{h}_4(\boldsymbol{X}) & L_{g_6}L_f\boldsymbol{h}_4(\boldsymbol{X}) \\ L_{g_1}L_f\boldsymbol{h}_5(\boldsymbol{X}) & L_{g_2}L_f\boldsymbol{h}_5(\boldsymbol{X}) & L_{g_3}L_f\boldsymbol{h}_5(\boldsymbol{X}) & L_{g_4}L_f\boldsymbol{h}_5(\boldsymbol{X}) & L_{g_5}L_f\boldsymbol{h}_5(\boldsymbol{X}) & L_{g_6}L_f\boldsymbol{h}_5(\boldsymbol{X}) \\ L_{g_1}L_f\boldsymbol{h}_6(\boldsymbol{X}) & L_{g_2}L_f\boldsymbol{h}_6(\boldsymbol{X}) & L_{g_3}L_f\boldsymbol{h}_6(\boldsymbol{X}) & L_{g_4}L_f\boldsymbol{h}_6(\boldsymbol{X}) & L_{g_5}L_f\boldsymbol{h}_6(\boldsymbol{X}) & L_{g_6}L_f\boldsymbol{h}_6(\boldsymbol{X}) \end{bmatrix}$$

$$= \begin{bmatrix} \frac{K_i}{m}+a & \frac{K_i}{m}-a & -\frac{K_i l_m^2 \cos^2 x_5}{2\lambda_2}+\frac{K_i l_m^2}{2J_{gx}} & \frac{K_i l_m^2 \cos^2 x_5}{2\lambda_2}-\frac{K_i l_m^2}{2J_{gx}} & \frac{\sqrt{2} l_m K_{igx}}{2J_{gx}} & -\frac{\sqrt{2}\cos x_5 l_m K_{ijy}}{2\lambda_2} \\ \frac{K_i}{m}-a & \frac{K_i}{m}+a & \frac{K_i l_m^2 \cos^2 x_5}{2\lambda_2}-\frac{K_i l_m^2}{2J_{gx}} & -\frac{K_i l_m^2 \cos^2 x_5}{2\lambda_2}+\frac{K_i l_m^2}{2J_{gx}} & -\frac{\sqrt{2} l_m K_{igx}}{2J_{gx}} & \frac{\sqrt{2}\cos x_5 l_m K_{ijy}}{2\lambda_2} \\ -\frac{K_i l_m^2 \cos^2 x_5}{2\lambda_2}+\frac{K_i l_m^2}{2J_{gx}} & \frac{K_i l_m^2 \cos^2 x_5}{2\lambda_2}-\frac{K_i l_m^2}{2J_{gx}} & \frac{K_i}{m}+a & \frac{K_i}{m}-a & \frac{\sqrt{2} l_m K_{igx}}{2J_{gx}} & \frac{\sqrt{2}\cos x_5 l_m K_{ijy}}{2\lambda_2} \\ \frac{K_i l_m^2 \cos^2 x_5}{2\lambda_2}-\frac{K_i l_m^2}{2J_{gx}} & -\frac{K_i l_m^2 \cos^2 x_5}{2\lambda_2}+\frac{K_i l_m^2}{2J_{gx}} & \frac{K_i}{m}-a & \frac{K_i}{m}+a & -\frac{\sqrt{2} l_m K_{igx}}{2J_{gx}} & -\frac{\sqrt{2}\cos x_5 l_m K_{ijy}}{2\lambda_2} \\ \frac{\sqrt{2} K_i l_m}{2J_{gx}} & -\frac{\sqrt{2} K_i l_m}{2J_{gx}} & \frac{\sqrt{2} K_i l_m}{2J_{gx}} & -\frac{\sqrt{2} K_i l_m}{2J_{gx}} & \frac{K_{igx}}{J_{gx}} & 0 \\ -\frac{\sqrt{2} K_i l_m \cos x_5}{2\lambda_2} & \frac{\sqrt{2} K_i l_m \cos x_5}{2\lambda_2} & \frac{\sqrt{2} K_i l_m \cos x_5}{2\lambda_2} & -\frac{\sqrt{2} K_i l_m \cos x_5}{2\lambda_2} & 0 & \frac{K_{ijy}}{\lambda_2} \end{bmatrix};$$

$$\boldsymbol{B}(\boldsymbol{X}) = \begin{bmatrix} \frac{2K_h x_1}{m} + l_m\left(\frac{2K_h l_m^2 x_4 + \Pi_3 - \Pi_4}{J_{rr}}\right) \\ \frac{2K_h x_1}{m} - l_m\left(\frac{2K_h l_m^2 x_4 + \Pi_3 - \Pi_4}{J_{rr}}\right) \\ \frac{2K_h x_2}{m} - l_m\left(\frac{2K_h l_m^2 x_3 - \Pi_1 - \Pi_2}{J_{rr}}\right) \\ \frac{2K_h x_2}{m} + l_m\left(\frac{2K_h l_m^2 x_3 - \Pi_1 - \Pi_2}{J_{rr}}\right) \\ \frac{\lambda_3 - \sqrt{2} K_h l_m^2 (x_3 - x_4)}{J_{gx}} \\ \frac{\lambda_1 - \sqrt{2} K_h l_m^2 (x_3 + x_4)\cos x_5}{\lambda_2} \end{bmatrix}$$

where $a = \frac{K_i l_m^2}{J_{rr}} + \frac{K_i l_m^2 \cos^2 x_5}{2\lambda_2} + \frac{K_i l_m^2}{2J_{gx}}$.

References

1. Han BC, Zheng SQ, Wang X, Yuan Q. Integral design and analysis of passive magnetic bearing and active radial magnetic bearing for agile satellite application. *IEEE Trans Magn* 2012;**48**(6):1959–66.
2. Fang JC, Li HT, Han BC. Torque ripple reduction in BLDC torque motor with nonideal back EMF. *IEEE Trans Power Electr* 2012;**27**(11):4630–7.
3. Fang JC, Zheng SQ, Han BC. Attitude sensing and dynamic decoupling based on active magnetic bearing of MSDGCMG. *IEEE Trans Instrum Meas* 2012;**61**(2):338–44.
4. Fang JC, Zheng SQ, Han BC. AMB vibration control for structural resonance of double-gimbal control moment gyro with high-speed magnetically suspended rotor. *IEEE/ASME Trans Mech* 2013;**18**(1):32–43.
5. Brown GV, Kascak A, Jansen RH, Dever TP, Duffy KP. Stabilizing gyroscopic modes in magnetic bearing supported flywheels by using cross-axis proportional gains. In: *AIAA guidance, navigation and control conference and exhibit, San Francisco*; 2005. Report No. AIAA-2005-5955.
6. Wei T, Fang JC. Research on the angular rate feedback control method for inhibition of moving gimbal effect of magnetically

suspended control moment gyroscope. *J Astron* 2005;**26**(1):19–23 [Chinese].
7. Wei T, Fang JC. Moving-gimbal effects compensation of double gimbal magnetically suspended control moment gyroscope based on compound control. *J Mech Eng* 2010;**46**(2): 159–65 [Chinese].
8. Liu HB, Li SY, Chai TY. Intelligent decoupling control of power plant main steam pressure and power output. *Int J Elec Power* 2003;**25**(10):809–901.
9. Dong DF, Meng XF, Liang F. Decoupling control of double-level dynamic vacuum system based on neural networks and prediction principle. *Vacuum* 2011;**86**(2):218–25.
10. Chai TY, Zhai LF, Yue H. Multiple models and neural networks based decoupling control of ball mill coal-pulverizing systems. *J Process Contr* 2011;**21**(3):351–66.
11. Wu ZL, Wang XL, Ge BM. Radial suspending control for magnetic suspending switched reluctance motor based on bp neural network. *Energy Proc* 2011;**13**:1248–55.
12. de Silva CW. Zadeh–macfarlane–jamshidi theorems on decoupling of a fuzzy rule base. *Sci Iran* 2011;**18**(3):611–6.
13. Chien T, Chen C. Control of AMIRA's ball and beam system via improved fuzzy feedback linearization approach. *Appl Math Model* 2010;**34**(12):3791–804.
14. Li-TzuuHseng S, Huang CJ, Chen CC. Novel fuzzy feedback linearization strategy for control via differential geometry approach. *ISA Trans* 2010;**49**(3):348–57.
15. Abootorabi-Zarchi H, Arab-Markadeh GhR, Soltani J. Direct torque and flux regulation of synchronous reluctance motor drives based on input-output feedback linearization. *Energ Convers Manage* 2010;**51**(1):71–80.
16. Hsu CT, Chen SL. Nonlinear control of a 3-pole active magnetic bearing system. *Automatica* 2003;**39**(2):291–8.
17. Zhu HQ, Zhou Y, Li TB, Liu XX. Decoupling control of 5 degrees of freedom bearingless induction motors using α-th order inverse system method. *Acta Autom Sinica* 2007;**33**(3):273–8.
18. Hung JY, Albritton NG, Xia F. Nonlinear control of a magnetic bearing system. *Mechatronics* 2003;**13**(6):621–37.
19. Yang YF, Ruan Y, Zhang WY, Wang Q, Yang ZB, Zhu HQ. Decoupling control of 5 degrees of freedom AC hybrid magnetic bearings based on inverse system. In: *Proceedings of the 30th Chinese control conference*; 2011. p. 278–282.
20. Fang JC, Ren Y. High-precision control for a single-gimbal magnetically suspended control moment gyro based on inverse system method. *IEEE Trans Ind Electron* 2011; **58**(9):4331–42.
21. Wu F, Zhang X, Ju P. Sterling Michael H. Decentralized nonlinear control of wind turbine with doubly fed induction generator. *IEEE Trans Power Syst* 2008;**23**(2):613–21.
22. Ren Y, Fang JC. Current-sensing resistor design to include current derivative in PWM H-bridge unipolar switching power amplifier for magnetic bearings. *IEEE Trans Ind Electron* 2012;**59**(12): 4590–600.
23. Fang JC, Ren Y. Self-adaptive phase-lead compensation based on unsymmetrical current sampling resistance network for magnetic bearing switching power amplifiers. *IEEE Trans Ind Electron* 2012;**59**(2):1218–27.